Lipid Bilayer Mechanics in a Pipette with Glass-Bilayer Adhesion

Tristan Ursell, Ashutosh Agrawal, and Rob Phillips*
Department of Applied Physics, California Institute of Technology, Pasadena, California

ABSTRACT Electrophysiology is a central tool for measuring how different driving forces (e.g., ligand concentration, transmembrane voltage, or lateral tension) cause a channel protein to gate. Upon formation of the high resistance seal between a lipid bilayer and a glass pipette, the so-called "giga-seal", channel activity can be recorded electrically. In this article, we explore the implications of giga-seal formation on the mechanical state of a lipid bilayer patch. We use a mechanical model for the free energy of bilayer geometry in the presence of glass-bilayer adhesion to draw three potentially important conclusions. First, we use our adhesion model to derive an explicit relationship between applied pressure and patch shape that is consistent with the Laplace-Young Law, giving an alternative method of calculating patch tension under pressure. With knowledge of the adhesion constant, which we find to be in the range ~0.4–4 mN/m, and the pipette size, one can precisely calculate the patch tension as a function of pressure, without the difficultly of obtaining an optical measurement of the bilayer radius of curvature. Second, we use data from previous electrophysiological experiments to show that over a wide range of lipids, the resting tension on a electrophysiological patch is highly variable and can be 10–100 times higher than estimates of the tension in a typical cell membrane. This suggests that electrophysiological experiments may be systematically altering channel-gating characteristics and querying the channels under conditions that are not the same as their physiological counterparts. Third, we show that reversible adhesion leads to a predictable change in the population response of gating channels in a bilayer patch.

INTRODUCTION

The use of pipettes to hold and deform both model and biological membranes is a key part of the experimental repertoire of modern membrane biophysics (1–6). Electrophysiology is a powerful and well-accepted technique for the quantification of ion channel gating in a variety of chemical and physical settings (7–10). In some cases, the set of possible ion channel conformations depends both on which molecules are present (e.g., ligands) and the physical state of the bilayer (e.g., bilayer thickness, curvature, or lateral tension) (11). In particular, some channels uniquely respond to their physical environment, and furthermore, it has been argued that lateral tension affects the gating of any ion channel that changes its areal footprint or hydrophobic thickness during a conformational change (8,12–14). Likewise, extreme conditions (e.g., very high salt concentration, very stiff bilayers, or high lateral tension) might cause some physiologically relevant channel conformations to be disfavored, while favoring conformations that are not usually adopted under physiological circumstances.

With these facts in mind, this article examines how the intrinsic interaction between a lipid bilayer and glass leads to resting tensions within a pipette that can be one or two orders-of-magnitude higher than the resting tension on a typical living cell membrane (15). Using linear elasticity theory, we calculate the bilayer patch shape and lateral tension in the presence of an applied suction pressure in the pipette. These calculations reveal a route to determine bilayer tension without knowledge of patch curvature. We compare this calculation with previous experimental results, which suggests that there is a relatively large variability in the strength of bilayer-glass adhesion, and hence a large variability in the resting tension on the bilayer during electrophysiological experiments.

BILAYER TENSION DURING GIGA-SEAL FORMATION

As a prerequisite to calculating the relationships among pressure, bilayer geometry, and tension, we first calculate the resting tension on a bilayer that has adhered to a glass pipette in the absence of an applied suction pressure. In all of the calculations that follow in this article, we make a number of simplifying mechanical assumptions about the bilayer: First, we assume that the behavior of the system is determined by lipid bilayer mechanics alone; we do not account for the effects of any structural or cytoskeletal components. Second, we assume that there are no folds, ripples, or extraneous sources of lipids that affect the smooth and uniform adhesion of the bilayer along the glass. Third, for the magnitudes of adhesion strength and pressure considered here, we assume that the contributions to bilayer energetics from mean curvature bending are negligible, an assumption that is explored in the Discussion. Fourth, we assume that the bilayer is a linear elastic material that has a stretch modulus K_A, and a linear relationship between the areal strain, ϕ, and the lateral tension, τ, given by $\tau = K_A\phi$. Fifth, we assume that adhesion between the glass and the bilayer is a reversible process that lowers the mechanical free energy. Finally, we assume that the tension in the adhered and freestanding regions is equal, but that

Submitted March 11, 2011, and accepted for publication August 30, 2011.

*Correspondence: phillips@pboc.caltech.edu

Editor: Reinhard Lipowsky.

0006-3495/11/10/1913/8 $2.00

doi: 10.1016/j.bpj.2011.08.057

adhesion results in a static friction between the glass and the bilayer that prevents sliding.

For the purposes of discussion, we consider a right cylindrical pipette as shown in Fig. 1. However, we emphasize that for all of the analysis that follows, our calculations apply to any pipette shape, so long as the radius is constant in the region where the bilayer transitions from the adhered region to the freestanding region (e.g., a cylindrical pipette with a tapered or bent tip). We construct an unstressed reference area, A_o, which simplifies the task of tracking how lipids partition themselves between the adhered and freestanding regions, but whose actual value has no effect on the outcome of the calculations. We define the adhered region as the domain adhered to the interior of the pipette, and we define the freestanding region as the circular domain with radius R_p. The reference area relates the freestanding and adhered region areas under equal stress, where the strain in the bilayer is related to these three areas by

$$A_o(1+\phi) = A_{\text{adh}} + \pi R_p^2, \tag{1}$$

with A_{adh} being the area of the adhered region. The stress and corresponding areal strain in the bilayer, ϕ, stores an elastic stretch energy

$$G_{\text{str}} = A_o \frac{K_A}{2}\phi^2. \tag{2}$$

Glass-bilayer adhesion is incorporated into the model through a phenomenological energy $G_{\text{adh}} = -\gamma A_{\text{adh}}$, where γ is the strength of adhesion and $A_{\text{adh}} = 2\pi R_p L_o$ for the particular bilayer configuration shown in Fig. 1 *A*. The adhesion energy can be rewritten as

$$G_{\text{adh}} = -\gamma\left(A_o(1+\phi) - \pi R_p^2\right) \tag{3}$$

using Eq. 1, and hence does not depend on the shape of the adhered region so long as R_p remains constant. The total mechanical free energy is the sum of the bilayer stretch and adhesion energies, given by

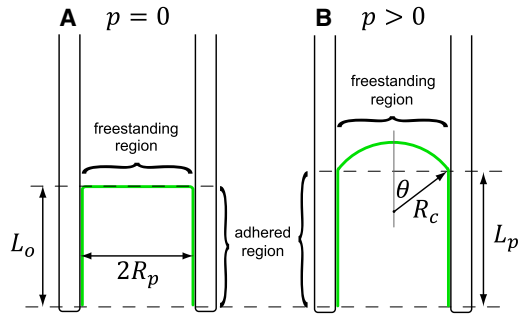

FIGURE 1 Schematic of pipette and bilayer geometry. The two figures illustrate the cases of (*A*) zero and (*B*) nonzero pressure, with the relevant geometric parameters for a cylindrical pipette. The bilayer is shown in green (color online)/gray.

$$G = G_{\text{str}} + G_{\text{adh}} = A_o\frac{K_A}{2}\phi^2 - \gamma\left(A_o(1+\phi) - \pi R_p^2\right). \tag{4}$$

Minimization of this energy with respect to the areal strain, ϕ, yields the equilibrium value $\phi = \gamma/K_A$, and hence the lateral tension $\tau = \gamma$ in both the adhered and freestanding bilayer regions, independent of the shape of the adhered region. This result shows that the resting lateral tension in the patch is determined only by the glass-bilayer adhesion strength, not by any geometric factors describing the patch or pipette, nor the amount of lipid bound to the glass. Later in this article we determine values for the adhesion coefficient, γ, which indicate that resting tensions due to adhesion may be orders-of-magnitude higher than the typical resting tension of a bilayer under physiological conditions.

BILAYER TENSION UNDER PRESSURE

When a pressure gradient is applied across the bilayer, the bilayer geometry changes to accommodate the energetic interplay between pressure and volume, such that the freestanding bilayer region adopts a domelike shape with a finite curvature (7,12), as shown in Fig. 1 *B*. We assume that this shape is described by a chord of a sphere, with a radius of curvature R_c and a polar angle θ, restricted by geometry to be

$$\theta = \sin^{-1}(\rho), \tag{5}$$

where the term in parentheses, $\rho = R_p/R_c$, is a dimensionless measure of the curvature for the freestanding spherical domain. In the limit of vanishing pressure, when the freestanding region tends toward a planar configuration, $R_c \to \infty$ and $\rho \to 0$. In contrast, for high values of applied pressure, when the freestanding bilayer tends toward a shape with maximum allowable curvature, $R_c \to R_p$ and $\rho \to 1$. For any shape that the freestanding region adopts between these two bounds, its area is given by

$$A_f = 2\pi R_c^2(1-\cos\theta) = \frac{2\pi R_p^2}{\rho^2}\left(1-\sqrt{1-\rho^2}\right). \tag{6}$$

The parameters that describe the bilayer shape can be related to the unstressed reference area and the areal strain, ϕ, felt throughout the bilayer in similar fashion to Eq. 1, by the relationship

$$(1+\phi)A_o = A_{\text{adh}} + \frac{2\pi R_p^2}{\rho^2}\left(1-\sqrt{1-\rho^2}\right), \tag{7}$$

where for the cylindrical pipette shown in Fig. 1 *B*, $A_{\text{adh}} = 2\pi R_p L_p$, with L_p as the length of the adhered region under pressure. Again, the shape of the adhered region is unimportant as long as R_p remains constant in the transition zone between the adhered and freestanding regions. A simple rearrangement of this equation gives an expression for the

adhered area as a function of areal strain, ϕ, and patch curvature, ρ. In addition to altering the amount of adhered area, the application of pressure increases the bilayer-enclosed volume relative to the zero-pressure state by an amount

$$\Delta V = \pi R_p^2\left(L_p - L_o\right) + \frac{\pi}{3}R_c^3(1-\cos\theta)^2(2+\cos\theta), \quad (8)$$

due to both bilayer areal strain and deformation of the freestanding region into a domelike shape. The values of L_o and L_p relate to the reference area, and affect where the transition between the freestanding and adhered zones is positioned within the pipette, but these parameters have no effect on the intrinsic mechanical state of the bilayer. Using Eqs. 5–7, Eq. 8 can be expressed as a function of the dimensionless curvature, ρ, and areal strain ϕ.

Incorporating the contributions from bilayer stretch, glass-bilayer adhesion, and pressure-volume coupling, the expression for the total bilayer free energy under pressure is

$$G(\phi,\rho) = A_o\frac{K_A}{2}\phi^2 - \gamma A_{\text{adh}}(\phi,\rho) - p\Delta V(\phi,\rho). \quad (9)$$

In contrast to the free energy at zero pressure, this free energy depends on two, independent variables, namely the areal strain, ϕ, and the dimensionless curvature ρ; whereas the pipette size R_p, pressure p, and adhesion constant γ are fixed parameters. In this situation, mechanical equilibrium is found by minimizing the free energy with respect to ϕ and ρ simultaneously.

Minimization of G with respect to ϕ yields the equilibrium value of the areal strain $\phi = (\gamma + pR/2)/K_A$. Multiplication of the areal strain with the stretch modulus gives the bilayer tension under pressure

$$\tau = \gamma + \frac{p\,R_p}{2}. \quad (10)$$

Equation 10 shows that the tension has a linear relationship to the adhesion strength, and has a separate linear dependence on the applied pressure. Note that the tension does not depend on the amount of adhered or freestanding area; the reference area; the radius of curvature of the freestanding region; or the position of the transition between the adhered and freestanding regions. This means that if one performs a set of calibration experiments to determine the glass-bilayer interaction energy (as discussed in Measuring Adhesion Strength from Bilayer Curvature), and then measures the pipette radius and the applied pressure, one knows the lateral tension without any measurements of patch curvature.

Minimization of the free energy in Eq. 9 with respect to the dimensionless curvature ρ yields two equations, one of which has the trivial solution $\rho = 0$, whereas the other equation gives

$$\rho = \frac{p\,R_p}{p\,R_p + 2\gamma}. \quad (11)$$

This equation makes a connection between the curvature of the freestanding region and applied pressure. Whereas normally, one must measure the curvature at each pressure to determine tension, we have derived a mechanical relationship that allows one to accurately calculate the curvature as a function of pressure. Conversely, one can rearrange this equation to

$$R_c = R_p + \frac{2\gamma}{p} \quad (12)$$

and use it as a tool to calibrate subsequent measurements. Specifically, by measuring the curvature of the freestanding region as a function of pressure, one can fit this equation to find the adhesion coefficient, γ, for a particular type of lipid and thus use Eq. 10 to find the tension in any subsequent experiment where the pipette size is known. Combining our Eqs. 10 and 12 yields the familiar Laplace-Young Law, $\tau = pR_c/2$, demonstrating that these are consistent formulations.

In addition to the dimensionless curvature ρ, the parameters in Eqs. 10 and 11 can be arranged to yield a dimensionless tension $\widehat{\tau} = \tau/\gamma$ and a dimensionless pressure $\widehat{p} = pR_p/2\gamma$. With these three dimensionless parameters, Eqs. 10 and 11 reduce to universal, parameter-free forms, given by

$$\widehat{\tau} = 1 + \widehat{p} \text{ and } \rho = \frac{\widehat{p}}{1+\widehat{p}}. \quad (13)$$

Fig. 2 shows plots of $\widehat{\tau}$ and ρ as a function of the dimensionless pressure $\widehat{p}$, to illustrate the functional form of these curves.

Our model also predicts that as pressure is applied and the domelike shape in the freestanding region appears, the bilayer stretches, and the proportion of lipids in the adhered region decreases, whereas the proportion of lipids in the

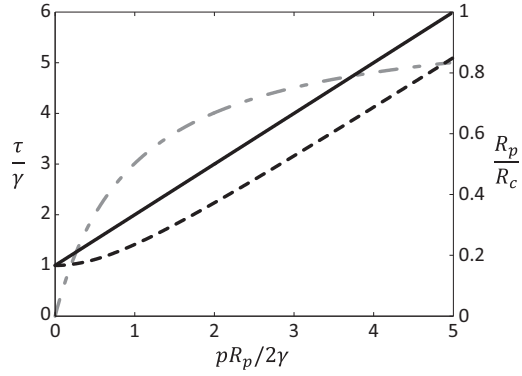

FIGURE 2 Plots showing the nondimensional variables under pressure. The dimensionless tension $\widehat{\tau} = \tau/\gamma$ for the method developed here (*solid line*, Method 3: $\tau = \gamma + pR_p/2$), and the method of Opsahl and Webb (20) (*dashed line*, Method 2: $\tau = \sqrt{(pR_p/2)^2 + \gamma^2}$), both of which do not require knowledge of bilayer curvature. (*Dot-dashed line*) Dimensionless curvature $\rho = R_p/R_c$ as a function of the dimensionless pressure $\widehat{p} = pR_p/2\gamma$, from Eq. 13.

freestanding region increases accordingly. We can couch this mathematically as the amount of lipid in the freestanding region at a given (dimensionless) pressure relative to the original amount of lipid in the freestanding region at zero pressure, given by

$$\Delta A_f = \frac{\left(\frac{A_f}{(1+\phi)}\right)\Big|_{\widehat{p}} - \left(\frac{A_f}{(1+\phi)}\right)\Big|_{\widehat{p}=0}}{\left(\frac{A_f}{(1+\phi)}\right)\Big|_{\widehat{p}=0}} = 2\frac{\left(\frac{(1+\widehat{p})}{\widehat{p}}\right)^2}{1+\widehat{p}\frac{\phi_o}{1+\phi_o}}\left(1-\sqrt{1-\left(\frac{\widehat{p}}{(1+\widehat{p})}\right)^2}\right) - 1, \quad (14)$$

where $\phi_o = \gamma/K_A \simeq 0.01$ (with $K_A \simeq 250$ mN/m (16)) is the areal strain of the bilayer at zero pressure, and the factor $1/(1+\phi)$ relates the stressed bilayer area to the unstressed area, and hence to the amount of lipid. This effect occurs because it is energetically favorable to remove lipids from the adhered region at a fixed cost per unit area, and add them to the dome-like, freestanding region where they increase the bilayer-enclosed volume that couples to the applied pressure, as shown in Fig. 3, *B* and *C*. This exchange of lipids from the adhered to the freestanding region is relatively small and hence should not affect the giga-Ohm seal resistance significantly. Experimental results suggest that within the same patch, freestanding bilayer height (17) and radius of curvature (7) are both reproducible aspects of bilayer geometry under pressure, and hence we expect this small exchange of lipids to be a reversible process.

For a fixed protein/lipid ratio, this increase in the amount of lipid in the freestanding region may also translate to a proportional increase in the amount of protein found in the freestanding region, and hence an increase in the number of measurable channels. In such a situation, the total number of channels as a function of applied pressure is given by

$$N(\widehat{p}) = c\frac{\pi R_p^2}{a_o(1+\phi_o)}(1+\Delta A_f), \quad (15)$$

where N is the number of channel proteins in the freestanding region, a_o is the area per lipid molecule, and c is the protein/lipid number ratio. At high pressures, where the areal strain is ~3–4%, this increase in freestanding bilayer, and the corresponding increase in measurable proteins, can be as large as ~20%, as shown in Fig. 3 *A*. For example, noninteracting channels that each individually have a dose-response as a function of pressure $P(\widehat{p})$, would have a population dose-response proportional to $N(\widehat{p})P(\widehat{p})$. Thus, in the absence of any mechanosensitivity of the channels themselves, a population of channels may exhibit a sensitivity to applied pressure, simply because the number of measurable channels increases as pressure increases.

MEASURING ADHESION STRENGTH FROM BILAYER CURVATURE

Using data from distinct preparations of multiple lipid mixtures that link curvature of the freestanding region to applied pressure, we calculated the glass-bilayer adhesion energy, γ, though as is evident below, the adhesion strength shows significant variation from one preparation to another. As part of their study to understand the gating of the mechanosensitive channel MscL (7), Moe and Blount obtained detailed measurements of patch curvature as a function of applied pressure. They measured the freestanding bilayer shape and channel electrical response on the same patch multiple times, confirming that both bilayer shape in the pipette and channel response to pressure are reproducible and reversible phenomena. Their data can be used to fit Eq. 12 for the adhesion energy and the pipette radius R_p. Ideally, if all pipettes and lipid preparations were identical, all of the lines associated with a particular lipid type would have the same slope, and only the pipette radius would

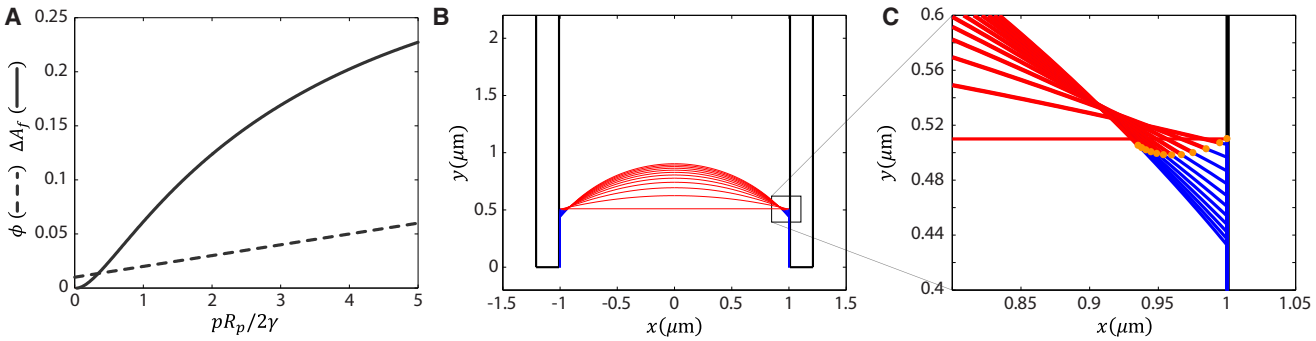

FIGURE 3 Plots showing freestanding area with dimensionless pressure. (*A*) The fractional change of lipid in the freestanding region as a function of dimensionless pressure, for $\phi_o = 0.01$. Under pressure, the freestanding region may gain up to ~20% more lipid. For reference, the areal strain of the bilayer is shown (*dashed line*). (*B*) Precise schematic of bilayer shape evolution under pressure, for a cylindrical pipette with $R_p = 1$ μm and $A_o = 2\pi R_p{}^2$. (*Red region* (color online)) Lipids originally in the freestanding region at zero pressure. (*C*) Zoom-in of box in panel *b* showing bilayer moving from the adhered region into the freestanding region.

change from one experiment to the next. However, the variability in our fits suggests that things may not be so simple. There are a number of potential ways that the interaction between glass and bilayer may be altered: for example, pH drift in the recording buffer (18,19), slight variations in glass composition and surface roughness, or changes in adhered lipid composition.

We performed this linear fit on the data to extract the adhesion energy for the different lipid mixtures. Our fitting results are summarized in Figs. 4 and 5. Some lipid mixtures show fairly homogeneous values of the adhesion energy, whereas others span a factor of two or three. Across all lipid types, the mean bilayer-glass adhesion energy was estimated to be 2.2 ± 1.2 mN/m. In a similar study, Opsahl and Webb (20) also reported values with a wide range of $\gamma = 0.5$–4 mN/m. Interestingly, when using the data published in their article, our model gives a slightly different result. Specifically, from their Fig. 3, they calculate $\gamma = 2.6$ mN/m, whereas we calculate $\gamma = 1.9$ mN/m. This difference stems from the way Opsahl and Webb incorporate the effects of adhesion into their model. They assume that the adhesion force, which acts normal to the contact surface, has a maximum value T_a. At the point of contact between the freestanding region and the pipette, this maximal force in the adhered region is balanced by the component of the tension in the freestanding region that acts perpendicular to the pipette surface. This force balance equation, along with the Laplace-Young Law for the freestanding region and a geometric relation similar to Eq. 5, results in the relationship

$$R_c^2 = R_p^2 + \frac{4T_a^2}{p^2}. \tag{16}$$

To make a comparison with this expression, we square the two sides of Eq. 12 to obtain

$$R_c^2 = R_p^2 + \frac{4\,\gamma^2}{p^2} + \frac{4\,\gamma R_p}{p}. \tag{17}$$

Considering γ equal to T_a, the difference between the two relations is restricted to the term $4\gamma\ R_p/p$. We can use the same dimensionless parameters used previously to illuminate the differences between these two methods. As noted earlier, this work found that the dimensionless tension and pressure were related by $\widehat{\tau} = 1 + \widehat{p}$, whereas Opsahl and Webb find that $\widehat{\tau} = \sqrt{1 + \widehat{p}^2}$. The differences in these two formulations are shown in Fig. 2. Numerically, these analytic differences seem significant, especially at intermediate pressures $1/2 \lesssim \widehat{p} \lesssim 3/2$.

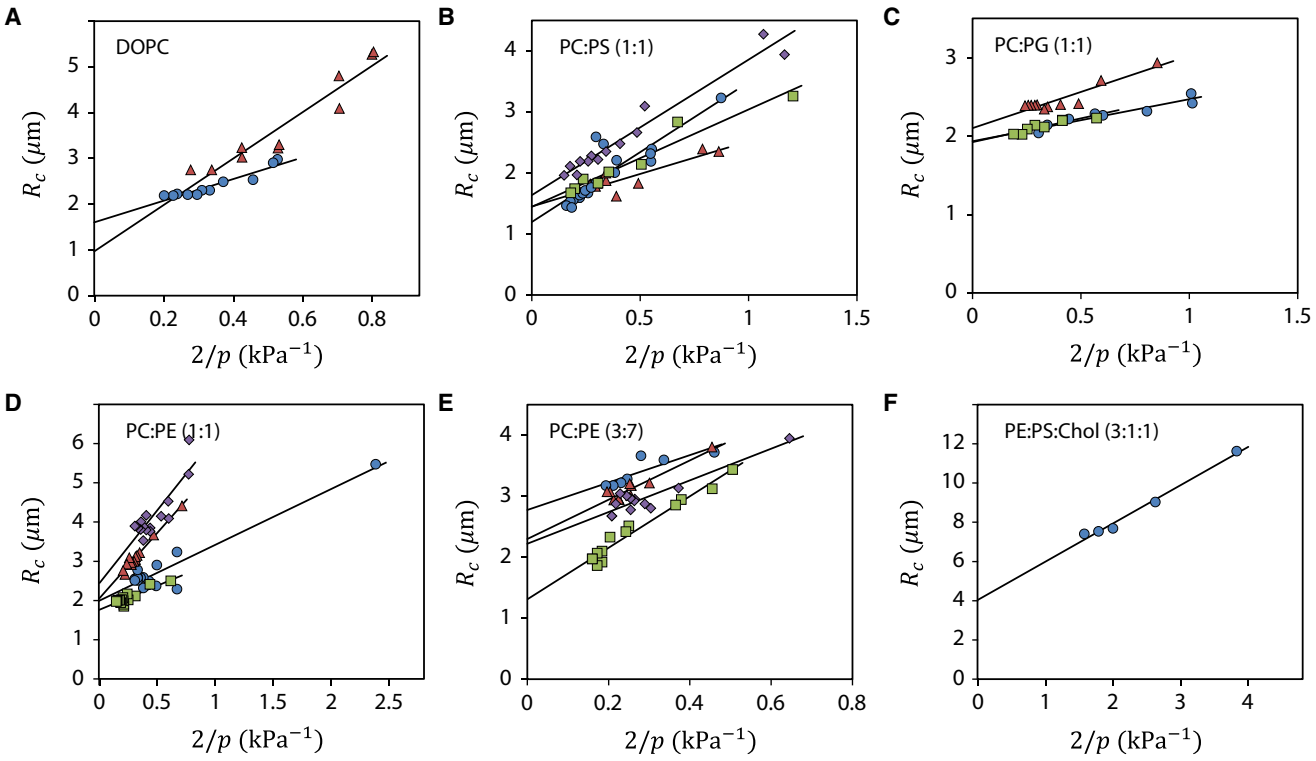

FIGURE 4 Glass-bilayer adhesion measured in different bilayer mixtures. Measurements of patch curvature as a function of applied pressure can be fit to Eq. 12 to find values of the adhesion energy, γ, from the slopes of the lines. Within a lipid mixture, variations in adhesion strength may be due to differences in pipette glass or buffer conditions (18). Between lipid mixtures, variations may be due to headgroup chemistry. Graphs *A–E* use data from Moe and Blount (7); graph *F* uses data from Opsahl and Webb (20). The different colors/symbols in each plot correspond to distinct data sets for a particular lipid type.

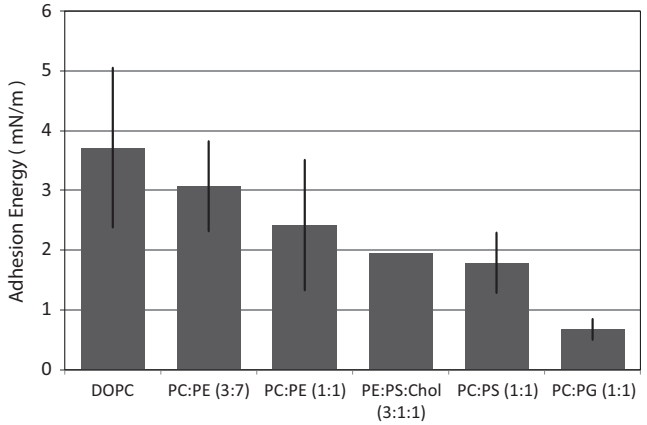

FIGURE 5 Bar graph comparing the strength of adhesion between the different lipid mixtures shown in Fig. 4. The means and standard deviations come from the linear slopes of the fits to each data set. The lipid mixtures are indicated on the x axis.

APPLICATIONS TO MECHANOSENSITIVE CHANNELS

In patch-clamp experiments with reconstituted mechanosensitive channels, varying the pressure across the bilayer results in increased tension that gates the channels. Both theoretical models and careful experimental studies have successfully established the functional dependence of channel gating on the tension in the lipid bilayer. However, to further our understanding of the gating mechanisms of these channels, it would be useful to connect the applied pressure to the corresponding tension in the bilayer without the tedious imaging usually required to measure the curvature of the freestanding region. To this end, below we examine available data from the experiments on mechanosensitive channels using 1), the Laplace-Young Law, 2), the formulation of Opsahl and Webb, 3), and the formulation developed in this work.

Method 1

As shown earlier, the two equilibrium Eqs. 10 and 12 obtained from energy minimization together yield the Young-Laplace relation, $\tau = pR_c/2$, for the freestanding bilayer region. If the bilayer curvature is known along with the pressure, this relation provides the most straightforward approach to compute the lateral tension. In their study of MscL gating, Moe and Blount (7) used the Laplace-Young Law to calculate the gating probability of the channel as a function of bilayer tension. However, in general, due to the challenges associated with obtaining optical data on the bilayer curvature, this approach has limited applicability.

Method 2

If optical data of bilayer curvature are lacking, the approach of Opsahl and Webb (20) can be used to calculate the radius of curvature of the freestanding bilayer region. As discussed in Measuring Adhesion Strength from Bilayer Curvature, the radius of curvature is given by

$$R_c = \sqrt{\frac{R_p^2 + 4\gamma^2}{p^2}},$$

and substituting this expression into the Young-Laplace relation yields

$$\tau = \sqrt{\gamma^2 + \left(\frac{pR_p}{2}\right)^2}.$$

Thus, with knowledge of the pipette radius and the adhesion energy, one can calculate the bilayer tension from this expression.

Method 3

For the same scenario where the curvature of the freestanding region is not known, a measure of the tension can be obtained from Eq. 10, $\tau = \gamma + pR_p/2$, derived earlier. This is equivalent to the substitution of Eq. 12 into the Young-Laplace relation. Similar to Method 2, an estimate of the adhesion energy and the pipette radius are required to calculate bilayer tension. However, in contrast to the relation presented in Method 2, in this method tension exhibits a linear dependence on adhesion energy, pipette size, and pressure, and is hence numerically distinct.

Comparing the tensions calculated from Method 2 ($\widehat{\tau}_2$) and Method 3 ($\widehat{\tau}_3$), we note that for higher values of $\widehat{p}$ both methods increase in a manner $\propto \widehat{p}$, as shown in Fig. 2, and the relative difference in tension between the two methods, $2(\widehat{\tau}_2 - \widehat{\tau}_3)/(\widehat{\tau}_2 + \widehat{\tau}_3)$, has a maximum at $\widehat{p} = 1$ of ~0.34, and then decreases like $\widehat{p}^{-1}$. We use the approaches discussed above to estimate the gating tension of the mechanosensitive channel of large conductance (MscL) from experiments that use three different lipid bilayers: PC16, PC18, and PC20, with acyl chain lengths of 16, 18, and 20 carbons, respectively. This study by Perozo et al. (10) estimated the applied pressure for the opening of a MscL channel to be ~24 mm Hg, 42 mm Hg, and 72.7 mm Hg, respectively. Due to the lack of available data on bilayer curvature, we use Methods 2 and 3 to estimate the gating tensions for the three different lipid types, and present these results in Table 1. To make these

TABLE 1 Estimation of gating tension (in mN/m) for Method 2 (Opsahl and Webb (20)) and Method 3 (this work) using data from Perozo et al. (10)

Pressure (mm Hg)	Method 1 $\tau = pR_c/2$	Method 2 $\tau = \sqrt{\gamma^2 + (pR_p/2)^2}$	Method 3 $\tau = \gamma + pR_p/2$
24	NA	4.1	5.3
42	NA	4.7	6.5
72.7	NA	6.1	8.7

NA = not available.

estimates, we assume an average adhesion energy of 3.7 mN/m for pure PC bilayers, as suggested by Fig. 5, and a pipette radius of 1 μm. For comparison, Moe and Blount (7) estimated the gating tension at ~10 mN/m for a MscL channel reconstituted in a DOPC/DOPS (1:1) bilayer.

DISCUSSION

Although a general consensus about the value of resting tension in cell membranes is lacking, a few studies have estimated it to be in the range of ~0.004–0.04 mN/m (15,21,22). On average, we calculated the tension induced by glass-bilayer adhesion to be ~2 mN/m. Thus, our work indicates that channel proteins reconstituted into lipid bilayers that are adhered to a pipette are subject to lateral tensions significantly higher than those found in cell membranes. Considering that many channels that were thought to be strictly voltage-gated channels respond in a nontrivial way to tension (8,14,23,24), and the fact that tension has been shown to alter the available conformational states of some channels (25), we wonder whether this large resting tension in patch-clamp experiments relative to those found in cells is systematically affecting a broad class of electrophysiological measurements.

In this work, we used linear elasticity to calculate the tension in a lipid bilayer adhered onto a glass pipette. For simplicity, we neglected the contribution of bending energy to the total system energy. A simple comparison of the orders of magnitude of the different energies justifies this approximation. For the case of vanishing applied pressure, an estimate of the increase in adhesion energy per unit unstressed area is $-\gamma\phi$, which is ~ -0.02 mN/m for $\gamma \approx 2$ mN/m. The increase in stretch energy per unit initial area is given by $K_A\phi^2/2$ and is calculated to be ~0.01 mN/m for $K_A \approx 250$ mN/m (16). The bending energy of the bilayer per unit area is given by $2\kappa_b H^2$, where κ_b is the bending modulus of the bilayer. The cylindrical section has a mean curvature of $H = 1/2R_p$ whereas the spherical patch has a maximum mean curvature of $H = 1/R_p$, and hence, for a typical value of $\kappa_b \approx 10^{-19}$ J and $R_p \approx 1$ μm, these contributions are $\sim 10^{-5}$ mN/m, which is two orders-of-magnitude smaller than the adhesion and stretch energies, and hence can be safely neglected.

Our elastic model treats the bilayer as a single elastic element, when in fact it is composed of two distinct leaflets that are coupled together by hydrophobicity. This treatment is equivalent to saying that the two leaflets are elastically identical and strongly coupled together. The strength of leaflet coupling does not affect the adhesion strength of the outer leaflet to the glass, nor the way that pressure and volume of the domed shaped interact, because that is strictly a geometrical feature. Hence leaflet coupling does not affect our calculations of tension and shape through energy minimization. Weaker interleaflet coupling may result in an asymmetric distribution of the mean tension between the two leaflets.

The areal strain of a bilayer under arbitrary pressure can be calculated by knowing the stretch modulus, $K_A \simeq 250$ mN/m, and tension on the bilayer (Eq. 10). Using average values of the adhesion strength ($\gamma \simeq 2$ mN/m) and stretch modulus, the areal strain of the bilayer is ~1% at zero pressure. During electrophysiological experiments, the applied pressure is of ~1/10 of an atmosphere or $p \simeq 10$ kPa, and the pipette radius is ~1 μm, leading to an areal strain of ~2–3%. Although bilayer rupture is a stochastic process (26), the approximate maximum strain that a bilayer can typically endure is ~3–4% (27). Thus, in the presence of adhesion and pressure, the bilayer is in the vicinity of its failure point. In addition, studies have linked the strength of glass-bilayer adhesion to increased giga-seal resistance (18) and hence decreased noise in electrophysiological measurements. These facts suggest a fundamental trade-off between patch lifetime and measurement noise; patches that adhere more tightly to the glass form a better giga-seal but fail more quickly due to stochastic rupture. Likewise, Eq. 10 shows that a larger pipette radius generates higher areal strain and bilayer tension, thus enhancing the risk of bilayer rupture.

The topic of bilayer-substrate adhesion has been an area of lively research, and as such we conclude with a few related remarks to put this work into a larger context. Adhesion is often studied using constant volume vesicles where adhesion strength can be determined from vesicle shape constraints (28). However, in the setting of electrophysiology we have used the complementary constant pressure ensemble. Additionally, whereas bilayer adhesion is often mediated indirectly by proteins, the adhesion we consider here involves the binding of individual lipids to glass, and hence tends to be significantly stronger than protein-mediated adhesion. For example, Seifert and Lipowsky (29) modeled the morphology of vesicles weakly adhered to substrates with $\gamma \approx 10^{-6}$–10^{-5} mN/m, and Smith et al. (30) studied the pulling of tethers in vesicles adhered to rigid substrates for adhesion strengths at $\sim 10^{-3}$ mN/m. Experimentally, Smith et al. (31) used magnetic tweezers to study the force-deflection of vesicles with protein-mediated adhesion, finding $\gamma \approx 10^{-5}$ mN/m.

Our estimate of the average adhesion strength, as well as estimates from bilayers (20) and even from different types of cell surfaces (17), suggest that direct binding of lipid on glass is a significantly stronger form of adhesion, of $\sim\gamma \simeq 2$ mN/m. Furthermore, our calculations based on the experimental data of Perozo et al. (10), indicate that applied pressure and adhesion are each contributing approximately equally to the net tension required to gate certain mechanosensitive channels in electrophysiological experiments. The fact that the resting tension comprises a significant portion of the gating tension, even for large mechanosensitive channels (e.g., MscL), together with the

fundamental tradeoff between adhesion strength and measurement noise, indicates the existence of an electrophysiological blind spot. Any channel that has conformational changes sensitive to tensions $\leq \gamma \simeq 2$ mN/m would be inaccessible to electrophysiology, yet it is precisely this lower tension regime $\ll 2$ mN/m that seems physiologically relevant for a broad range of cellular membranes.

CONCLUSION

In this work we used a linear elastic model and data from previous experiments on mechanosensitive channels to gain a better understanding of how glass-bilayer adhesion affects the mechanical state of a bilayer patch during an electrophysiological experiment. We derived an alternative method for calculating bilayer tension that does not rely on imaging the bilayer, but does require knowledge of the adhesion strength and pipette size. We used this to calculate the adhesion strength across multiple lipid types and found that it is highly variable, and that adhesion causes the resting tension, in the absence of applied pressure, to be orders-of-magnitude higher than estimated physiological tensions.

Additionally, our calculations indicate that applied pressure augments the amount of lipid in the freestanding bilayer region, thus increasing the amount of measurable channel proteins during an experiment and, hence, imbuing every patch with a pressure-dependent response. Together, these insights should make it easier to measure and interpret the mechanical state of the bilayer, although they also suggest the existence of multiple sources of uncontrolled variation in apparent channel behavior during electrophysiological experiments.

We thank Paul Blount for kindly providing us with the bilayer shape data. The authors thank Rod MacKinnon and Daniel Schmidt for stimulating discussion and critical reading of the early manuscript, as well as helpful comments from an anonymous reviewer.

We are grateful for the following funding sources: T.U. for the Genentech Bio-X Postdoctoral Fellowship, and T.U., A.A., and R.P. for the National Institutes of Health Director's Pioneer Award, the Howard Hughes Medical Institute Collaborative Innovation Award, and National Institutes of Health Award R01 GM084211.

REFERENCES

1. Evans, E. A. 1983. Bending elastic modulus of red blood cell membrane derived from buckling instability in micropipet aspiration tests. *Biophys. J.* 43:27–30.
2. Evans, E., and A. Yeung. 1989. Apparent viscosity and cortical tension of blood granulocytes determined by micropipet aspiration. *Biophys. J.* 56:151–160.
3. Sit, P. S., A. A. Spector, …, W. E. Brownell. 1997. Micropipette aspiration on the outer hair cell lateral wall. *Biophys. J.* 72:2812–2819.
4. Guilak, F., J. R. Tedrow, and R. Burgkart. 2000. Viscoelastic properties of the cell nucleus. *Biochem. Biophys. Res. Commun.* 269:781–786.
5. Roux, A., D. Cuvelier, …, B. Goud. 2005. Role of curvature and phase transition in lipid sorting and fission of membrane tubules. *EMBO J.* 24:1537–1545.
6. Roux, A., G. Koster, …, P. Bassereau. 2010. Membrane curvature controls dynamin polymerization. *Proc. Natl. Acad. Sci. USA.* 107: 4141–4146.
7. Moe, P., and P. Blount. 2005. Assessment of potential stimuli for mechano-dependent gating of MscL: effects of pressure, tension, and lipid headgroups. *Biochemistry.* 44:12239–12244.
8. Schmidt, D., and R. MacKinnon. 2008. Voltage-dependent K^+ channel gating and voltage sensor toxin sensitivity depend on the mechanical state of the lipid membrane. *Proc. Natl. Acad. Sci. USA.* 105:19276–19281.
9. Suchyna, T. M., S. E. Tape, …, P. A. Gottlieb. 2004. Bilayer-dependent inhibition of mechanosensitive channels by neuroactive peptide enantiomers. *Nature.* 430:235–240.
10. Perozo, E., A. Kloda, …, B. Martinac. 2002. Physical principles underlying the transduction of bilayer deformation forces during mechanosensitive channel gating. *Nat. Struct. Biol.* 9:696–703.
11. Phillips, R., T. Ursell, …, P. Sens. 2009. Emerging roles for lipids in shaping membrane-protein function. *Nature.* 459:379–385.
12. Sukharev, S. I., W. J. Sigurdson, …, F. Sachs. 1999. Energetic and spatial parameters for gating of the bacterial large conductance mechanosensitive channel, MscL. *J. Gen. Physiol.* 113:525–540.
13. Wiggins, P., and R. Phillips. 2004. Analytic models for mechanotransduction: gating a mechanosensitive channel. *Proc. Natl. Acad. Sci. USA.* 101:4071–4076.
14. Morris, C. E., and P. F. Juranka. 2007. Lipid stress at play: mechanosensitivity of voltage-gated channels. *Curr. Top. Membr.* 49:298–338.
15. Morris, C. E., and U. Homann. 2001. Cell surface area regulation and membrane tension. *J. Membr. Biol.* 179:79–102.
16. Rawicz, W., K. C. Olbrich, …, E. Evans. 2000. Effect of chain length and unsaturation on elasticity of lipid bilayers. *Biophys. J.* 79:328–339.
17. Suchyna, T. M., V. S. Markin, and F. Sachs. 2009. Biophysics and structure of the patch and the gigaseal. *Biophys. J.* 97:738–747.
18. Priel, A., Z. Gil, …, S. D. Silberberg. 2007. Ionic requirements for membrane-glass adhesion and giga seal formation in patch-clamp recording. *Biophys. J.* 92:3893–3900.
19. Schönherr, H., J. M. Johnson, …, S. G. Boxer. 2004. Vesicle adsorption and lipid bilayer formation on glass studied by atomic force microscopy. *Langmuir.* 20:11600–11606.
20. Opsahl, L. R., and W. W. Webb. 1994. Lipid-glass adhesion in giga-sealed patch-clamped membranes. *Biophys. J.* 66:75–79.
21. Dai, J., and M. P. Sheetz. 1999. Membrane tether formation from blebbing cells. *Biophys. J.* 77:3363–3370.
22. Upadhyaya, A., and M. P. Sheetz. 2004. Tension in tubulovesicular networks of Golgi and endoplasmic reticulum membranes. *Biophys. J.* 86:2923–2928.
23. Gu, C. X., P. F. Juranka, and C. E. Morris. 2001. Stretch-activation and stretch-inactivation of *Shaker*-IR, a voltage-gated K^+ channel. *Biophys. J.* 80:2678–2693.
24. Morris, C. E., and P. F. Juranka. 2007. Nav channel mechanosensitivity: activation and inactivation accelerate reversibly with stretch. *Biophys. J.* 93:822–833.
25. Akitake, B., A. Anishkin, and S. Sukharev. 2005. The "dashpot" mechanism of stretch-dependent gating in MscS. *J. Gen. Physiol.* 125:143–154.
26. Evans, E., V. Heinrich, …, W. Rawicz. 2003. Dynamic tension spectroscopy and strength of biomembranes. *Biophys. J.* 85:2342–2350.
27. Boal, D. 2002. Mechanics of the Cell, 1st Ed. Cambridge University Press, New York, NY.
28. Evans, E. 1991. Entropy-driven tension in vesicle membranes and unbinding of adherent vesicles. *Langmuir.* 7:1900–1908.
29. Seifert, U., and R. Lipowsky. 1990. Adhesion of vesicles. *Phys. Rev. A.* 42:4768–4771.
30. Smith, A. S., E. Sackmann, and U. Seifert. 2004. Pulling tethers from adhered vesicles. *Phys. Rev. Lett.* 92:208101.
31. Smith, A. S., B. G. Lorz, …, E. Sackmann. 2006. Force-controlled equilibria of specific vesicle-substrate adhesion. *Biophys. J.* 90:L52–L54.